

Effects of hydrogen and bromide on the corrosion of spent nuclear fuel and γ -irradiated $\text{UO}_2(\text{s})$ in NaCl brine

By V. Metz*, A. Loida, E. Bohnert, D. Schild and K. Dardenne

Institut für Nukleare Entsorgung (INE), Forschungszentrum Karlsruhe, P.O. Box 3640, 76021 Karlsruhe, Germany

(Received October 16, 2007; accepted in revised form March 31, 2008)

*Spent nuclear fuel / Radiolysis /
Uranium dioxide corrosion / Hydrogen / Bromide*

Summary. Radiation induced $\text{UO}_2(\text{s})$ corrosion is studied at elevated hydrogen pressure in NaCl brine containing traces of bromide. Release of Sr, Cs, Tc and actinides was measured in corrosion experiments with spent nuclear fuel pellets in presence of 10^{-2} mol H_2 ($\text{kg H}_2\text{O}$) $^{-1}$, and 10^{-4} and 10^{-3} mol Br^- ($\text{kg H}_2\text{O}$) $^{-1}$, respectively. For comparison, depleted $\text{UO}_2(\text{s})$ pellets were γ -irradiated in NaCl brine at 10^{-3} mol H_2 ($\text{kg H}_2\text{O}$) $^{-1}$ and 0 – 10^{-4} mol Br^- ($\text{kg H}_2\text{O}$) $^{-1}$, respectively. In the γ -radiolysis experiments a significant increase in the yield of radiolytic products due to Br^- is observed. Both, in the γ -radiolysis experiment with Br^- and in that without Br^- , the $\text{UO}_2(\text{s})$ sample was oxidized, and the concentration of dissolved uranium was controlled by precipitation of meta-schoepite and clarkeite. In the spent nuclear fuel corrosion experiment under H_2 overpressure, aqueous concentrations of Tc and Np were in the range of solubilities of Tc(IV) and Np(IV) hydroxides, whereas measured U concentrations were between solubilities of U(VI) and U(IV) phases. The release rate of Sr was significantly increased in the presence of Br^- traces. Results of the complementary spent nuclear fuel corrosion and γ -radiolysis experiments allow the conclusion that Br^- traces reduce significantly the protective hydrogen effect with respect to the release of certain radionuclides and the yield of radiolytic products.

1. Introduction

The disposal in deep bedrock repositories is considered as the preferred option for the management of spent nuclear fuel, SNF, in many countries. Though, geological or geo-technical barrier system may prevent to some extent groundwater contacting the fuel, intrusion of solutions into disposal rooms has to be taken into account within the long-term safety case of a SNF repository. The fate of spent nuclear fuel and the associated release of radionuclides depend on SNF corrosion kinetics as well as on thermodynamics. The corrosion behavior of the fuel is influenced by a variety of factors such as radionuclide inventory, resulting α -, β - and γ -dose rates, availability of oxidizing radiolytic products, temperature, groundwater composition, pH and redox potential.

Radiolysis of aqueous solutions is accompanied by the formation of redox agents. With respect to primary radiolysis products, H_2 molecules and H^\bullet radicals are the main reductants, whereas the main oxidants are H_2O_2 (in an α -radiation field/high linear energy transfer, LET) and OH^\bullet radicals (in a β - and γ -radiation field/low LET) in aqueous solutions of low chloride concentration. In salt brines, H_2 molecules are the main reductants, whereas radiolytic oxidants are dominated by oxo-halogenides, such as HClO (both for high and low LET), OH^- (for high LET) and Cl_2^- (for low LET) [1]. Aqueous solution in contact with spent nuclear fuel could radiolytically produce oxidants which oxidize the relatively stable $\text{UO}_2(\text{s})$ matrix of SNF into much more soluble U(VI), as long as concentrations of inhibitors such as H_2 are sufficiently low [2–4]. As a consequence, matrix bound radionuclides, such as ^{90}Sr , ^{237}Np , ^{239}Pu and ^{241}Am , are released. Yet, within few years after solution intrusion into SNF repository, high hydrogen concentrations will be achieved in the near field of the fuel, mainly caused by anaerobic corrosion of Fe-based waste containers. Hydrogen remains dissolved as long as the pressure built-up in the disposal site does not exceed the minimal principal stress of the geological setting (*i.e.* hydrostatic or lithostatic pressure, respectively). SNF leaching tests and radiolysis experiments indicated that hydrogen both considerably inhibits corrosion of the $\text{UO}_2(\text{s})$ matrix and impedes radiolytic decomposition of the studied groundwater simulates [2–8]. Though bromide is a minor constituent in groundwater of deep geological formations, it is present in a concentration range relevant for radiolytic processes, *i.e.* up to 10^{-3} mol ($\text{kg H}_2\text{O}$) $^{-1}$ in granitic groundwater [9, 10], up to 10^{-4} mol ($\text{kg H}_2\text{O}$) $^{-1}$ in argillaceous porewater [11] and up to 10^{-1} mol ($\text{kg H}_2\text{O}$) $^{-1}$ in salt brines from deep salt formations [12–14]. It is known from radiolysis of water that even low concentrations of bromide compete with hydrogen for oxidative radiolytic products and consequently reduces the inhibition effect of hydrogen on radiolytic decomposition [15, 16]. Results of α - and γ -radiolysis experiments in NaCl brine demonstrate (i) it is not the major constituent Cl^- , but the presence of Br^- traces that dominates formation of radiolytic species [17], and (ii) Br^- concentrations of 10^{-4} to 10^{-3} mol ($\text{kg H}_2\text{O}$) $^{-1}$ considerably promote radiolytic decomposition, even at 10^{-2} mol H_2 ($\text{kg H}_2\text{O}$) $^{-1}$ [8, 16].

In two recent conference proceedings we reported first results of our experiments on the dependence of SNF corrosion and γ -radiolysis on Br^- concentration in solu-

* Author for correspondence (E-mail: volker@ine.fzk.de).

tion [16, 18]. The present study is a continuation of these experiments with the aim to determine whether the protective effect of non-radiolytic hydrogen is significantly reduced – if not annihilated – by bromide.

2. Materials and methods

We study radiation induced $\text{UO}_2(\text{s})$ dissolution in NaCl brine comprising both hydrogen and traces of bromide. Static experiments were conducted in closed reaction vessels in absence of $\text{CO}_2(\text{g})$ /dissolved inorganic carbon. Two types of experiments were performed:

(A) α -, β -, γ -radiation induced $\text{UO}_2(\text{s})$ corrosion: SNF pellet sized fragments with Zircalloy cladding were immersed in NaCl brine with bromide traces at room temperature in two experiments, (A)K18 and (A)K19. Under inert gas atmosphere, pellets of 6.6 g mass had been cut off from a fuel rod, having a burn-up of 50 MW d $(\text{kg U})^{-1}$, and stored in “gas-tight” containers since 1992. However, in the course of 13 years of storage, the fuel samples suffered pre-oxidation to some extent. During four wash cycles in two weeks, the instant release fraction (labile radionuclides such as *e.g.* ^{137}Cs) was partly removed from the fuel pellets before starting the static stage of the corrosion experiments. Results of wash cycles are published in [18]. For the static stage, Ti-Pd-lined stainless steel autoclaves (with a total volume of 500 mL per autoclave) were used. Both autoclaves were filled with 200 mL of 5.3 mol $(\text{kg H}_2\text{O})^{-1}$ NaCl solution, resulting in an initial mass to volume ratio $m/V = 0.033 \text{ g mL}^{-1}$. Solutions of experiments (A)K19 and (A)K18 contained 10^{-4} to 10^{-3} mol $\text{Br}^- (\text{kg H}_2\text{O})^{-1}$, respectively. By inserting 4 MPa of a 8 vol. % $\text{H}_2/92$ vol. % Ar gas mixture a hydrogen partial pressure of 0.32 MPa was achieved, corresponding to 10^{-2} mol $\text{H}_2 (\text{kg H}_2\text{O})^{-1}$. The pressure remained constant at 4 MPa during each leaching interval, until sampling of gases and solutions were performed. A solution aliquot of about 10 mL was taken at each sampling step. Between the 2nd and 3rd sampling (interval 212 to 282 d), a pure Ar overpressure of 0.1 MPa was applied. After the 3rd sampling the solution was completely replaced. According to calculations, a mean γ -dose rate of about 3 Gy h^{-1} was applied in the bulk solution of the autoclaves. Dose rates of α - and β -radiation in close vicinity of the fuel particles are by orders of magnitude higher than the γ -dose rate [19].

(B) γ -radiation induced $\text{UO}_2(\text{s})$ corrosion: Pellets of depleted $\text{UO}_2(\text{s})$ (0.2 g and 4×10^3 Bq per pellet, respectively) were γ -irradiated in 6 mol $(\text{kg H}_2\text{O})^{-1}$ NaCl solution at the GB77 ^{60}Co -source (Institut für Oberflächenmodifizierung, Leipzig, Germany). Experiment (B)L1_06 was conducted in 172 mL NaCl brine without bromide ($m/V = 1.2 \times 10^{-2} \text{ g mL}^{-1}$), experiment (B)L2_06 in 182 mL NaCl brine with 10^{-4} mol $\text{Br}^- (\text{kg H}_2\text{O})^{-1}$ ($m/V = 1.1 \times 10^{-2} \text{ g mL}^{-1}$). Both solutions contained initially 10^{-3} mol $\text{H}_2 (\text{kg H}_2\text{O})^{-1}$. The experiments were performed in autoclaves, manufactured from Ni-Cr-Mo-Fe-based Hastelloy, which were thermostated at 35 °C. About half of the autoclave volume was occupied by a bellow, which was pressurized with Ar. Unlike the SNF corrosion experiments, in experiments (B)L1_06 and (B)L2_06 the bellows trans-

mitted a pressure of 25 MPa onto the solutions, thereby forcing radiolysis gases to remain dissolved (no headspace). The mean γ -dose rate at the position of the autoclaves was measured with a Fricke dosimeter and varied between 300–400 Gy h^{-1} . Results of the production of radiolysis gases are published in [16]. In the blank experiment (B)LPI, another $\text{UO}_2(\text{s})$ sample, having the same characteristics as those of experiments (B)L2_06 and (B)L1_06, was immersed in bromide free 6 mol $(\text{kg H}_2\text{O})^{-1}$ NaCl. The blank experiment was not γ -irradiated, and the headspace of the autoclave was filled with argon. Before starting the experiments, all $\text{UO}_2(\text{s})$ pellets were annealed for three hours at 1150 °C in 5 vol. % $\text{H}_2/95$ vol. % Ar atmosphere, to ensure an initial U(IV) surface composition.

Solution and gas atmosphere were sampled four times during the static stage of the SNF corrosion experiments, at the end of the γ -radiolysis experiments and at the end of the blank experiment. Solution aliquots were filtered with ultrafilters of 1.8 nm pore size, except samples from the blank experiment. Solutions of experiments (A)K19 and (A)K18 were analyzed by α -spectrometry using a Canberra 74/01 analysis chamber with a S100 field channel analysator (^{238}Pu , $^{239/240}\text{Pu}$), γ -spectrometry using Ge-detectors Canberra EGC-15-185-R and Canberra GX3018 ($^{134/137}\text{Cs}$), liquid scintillation counting using a Packard Tri-Carb 2500 TR/AB LSC (^{90}Sr , ^{241}Pu) and with mass spectrometry using a ICP-MS Perkin Elmer ELAN 6100 (^{99}Tc , ^{237}Np , ^{238}U). In the final solutions of γ -radiolysis and blank experiments U concentrations were measured by ICP-MS. Concentrations of Cr, Fe, Ni and Mo in final solutions of γ -radiolysis were analyzed by optical emission spectrometry using a Perkin Elmer ICP-AES PE2000. The estimated accuracy of Cs and Sr concentrations was $\pm 10\%$. Inaccuracy of Np, Pu, Tc and U measurements was up to three times higher for concentrations close to the respective detection limits, *i.e.* 5×10^{-10} mol $(\text{kg H}_2\text{O})^{-1}$ for ^{237}Np , 1×10^{-10} mol $(\text{kg H}_2\text{O})^{-1}$ for $^{239/240}\text{Pu}$, ^{99}Tc and ^{238}U , and 1×10^{-12} mol $(\text{kg H}_2\text{O})^{-1}$ for ^{238}Pu . The analytical uncertainty of measured Cr, Fe, Mo, Ni and Zr concentrations was $\leq 5\%$. Compositions of the gas samples were analyzed using a Balzers-Pfeiffer GAM 400 quadrupole mass spectrometer. The pH of the solutions was measured using a ROSS semi-micro combination electrode and ORION pH meter 720-A. The estimated accuracy was ± 0.05 pH units. Conversion of measured pH values into H^+ concentrations ($-\log C(\text{H}^+) = \text{pH}_c$) was carried out according to the procedure described by Altmaier *et al.* [20]. To characterize secondary phases and oxidation state of uranium in corrosion layers, samples recovered from the radiolysis experiments were analyzed by means of AFM, EXAFS, SEM-EDS and XPS techniques. A Turbometrix Explorer AFM operating in contact mode was used for imaging the pellets' surfaces under ambient conditions in air (after drying). Surface sensitive grazing incidence (GI) U L_3 XAFS measurements were performed at the INE-beamline for actinide research, FZK Angströmquelle Karlsruhe, ANKA. Spectra of clarkeite, meta-schoepite and uraninite ($\text{UO}_2(\text{s})$) were recorded as references. Scanning electron microscope-energy disperse spectrometry (SEM-EDS) analyses were done, using a CamScan FE44 SEM equipped with a Noran EDS unit. XPS analyses were performed using a Physical

Electronics Inc. model 5600ci spectrometer equipped with a hemispherical capacitor analyzer and multichannel detector. Elemental lines were recorded by monochromatic Al K_{α} X-ray excitation (1486.6 eV).

3. Results

3.1 Release of Cs, Sr, Tc and actinides from corroding spent nuclear fuel

Aqueous concentrations of Cs, Sr, Np, Tc, Pu and U measured in experiments (A)K18 and (A)K19 are given in Table 1. The respective data of Cs, Sr, Pu and U are plotted as function of time in Fig. 1. Concentrations of Sr and Pu increased

by less than one order of magnitude in the 0 to 282 d interval, *i.e.* before replacement of the solution. In contrast to Sr and Pu, a decrease in U concentrations with time is observed. There is no clear trend in the Tc concentration pattern; Np concentrations were below detection limit except in one sampling. Before the replacement, Cs concentration was about constant with time; afterwards a significantly lower concentration was measured. With respect to release of Cs and Sr, there is no significant difference between results from (A)K18 and (A)K19, despite the difference in the initial bromide concentrations of the experiments (Fig. 1). However, concentrations of Pu and U were significantly higher in presence of 10^{-3} mol Br^- ($\text{kg H}_2\text{O}^{-1}$) (experiment (A)K18) compared to their concentrations in experiment (A)K19 with

Table 1. Experimental conditions, pHc values, gas compositions, aqueous concentrations of Cs, Sr, Tc, U, Np, Pu, U and Zr of SNF corrosion experiments (A)K18 and (A)K19. Concentrations of solutions filtered by ultrafilters with 1.8 nm pore size are given. “< d.l.” denotes below detection limit.

(A)K18 – 5.3 m NaCl/ 10^{-3} m Br^-				
time/d	56	212	282	777 ^a
P(H_2)/MPa	0.32	0.32	0 (Ar)	0.32
pH _c	7.8	7.0	7.5	7.6
Concentrations/mol ($\text{kg H}_2\text{O}^{-1}$)				
C(Cs)	5×10^{-6}	8×10^{-6}	5×10^{-6}	9×10^{-7}
C(Sr)	1×10^{-7}	3×10^{-7}	7×10^{-7}	2×10^{-7}
C(Pu)	2×10^{-10}	4×10^{-10}	1×10^{-9}	1×10^{-9}
C(U)	1×10^{-7}	1×10^{-8}	2×10^{-6}	7×10^{-9}
C(Tc)	8×10^{-9}	2×10^{-10}	2×10^{-8}	< d.l.
C(Np)	< d.l.	< d.l.	9×10^{-10}	< d.l.
C(Zr)	2×10^{-7}	1×10^{-6}	3×10^{-6}	1×10^{-8}
X(H_2)	7.76%	7.27%	n.d.	10.08%
X(O_2)	< d.l.	< d.l.	n.d.	< d.l.
X(Ar)	92.23%	92.72%	n.d.	89.90%
X(Kr)	< d.l.	0.001%	n.d.	0.001%
X(Xe)	0.002%	0.003%	n.d.	0.006%
X(CO_2)	< d.l.	< d.l.	n.d.	< d.l.
X(H_2)/X(Ar)	0.08	0.08	n.d.	0.11
(A)K19 – 5.3 m NaCl/ 10^{-4} m Br^-				
time/d	56	212	282	777 ^a
P(H_2)/MPa	0.32	0.32	0 (Ar)	0.32
pH _c	7.8	7.0	7.5	6.8
Concentrations/mol ($\text{kg H}_2\text{O}^{-1}$)				
C(Cs)	5×10^{-6}	6×10^{-6}	4×10^{-6}	1×10^{-6}
C(Sr)	2×10^{-7}	3×10^{-7}	5×10^{-7}	2×10^{-7}
C(Pu)	2×10^{-11}	3×10^{-11}	4×10^{-11}	3×10^{-10}
C(U)	3×10^{-8}	4×10^{-9}	6×10^{-8}	2×10^{-9}
C(Tc)	1×10^{-10}	2×10^{-9}	4×10^{-9}	< d.l.
C(Np)	< d.l.	< d.l.	< d.l.	< d.l.
C(Zr)	2×10^{-7}	1×10^{-6}	3×10^{-6}	6×10^{-9}
X(H_2)	7.58%	7.33%	n.d.	9.94%
X(O_2)	< d.l.	< d.l.	n.d.	< d.l.
X(Ar)	92.42%	92.66%	n.d.	90.06%
X(Kr)	< d.l.	< d.l.	n.d.	0.001%
X(Xe)	0.001%	0.002%	n.d.	0.003%
X(CO_2)	< d.l.	< d.l.	n.d.	< d.l.
X(H_2)/X(Ar)	0.08	0.08	n.d.	0.11

a: After 3rd sampling (282 d), solutions of both experiments were completely replaced. Bold values denote data taken from Loida *et al.* [18].

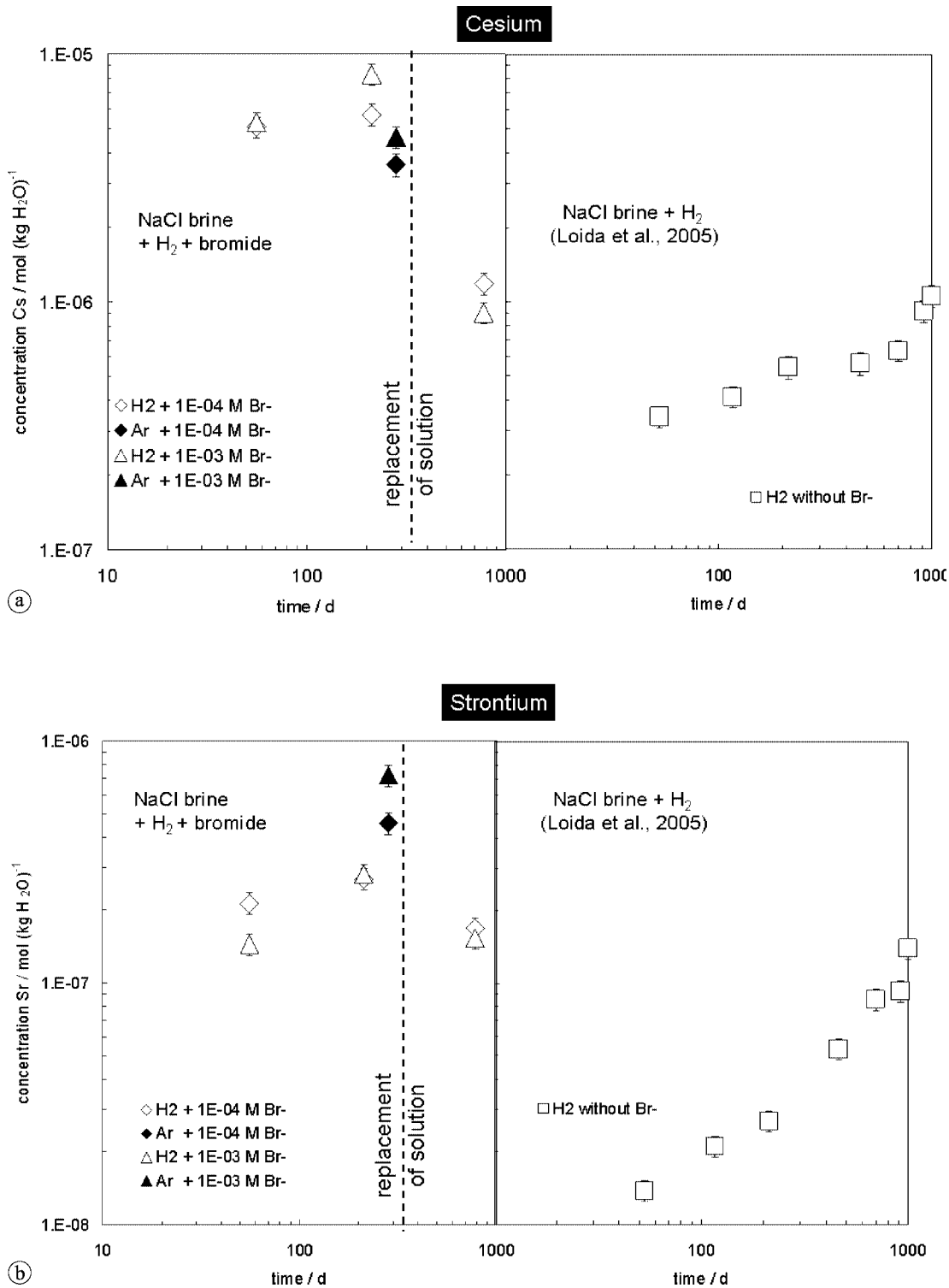


Fig. 1. Variation of aqueous concentrations of cesium (a), strontium (b), uranium (c) and plutonium (d) as function of time in SNF corrosion experiments in NaCl brine under an Ar/H₂ gas atmosphere. Results of experiments (A)K18 (containing 10⁻³ mol Br⁻ (kg H₂O)⁻¹) and (A)K19 (containing 10⁻⁴ mol Br⁻ (kg H₂O)⁻¹) are compared to those of an experiment without bromide, published by Loida *et al.* [7]. Open symbols denote concentrations measured under 0.32 MPa H₂ and 3.7 MPa Ar partial pressures; filled symbols denote concentrations under 0.1 MPa Ar gas atmosphere. Solutions of experiments (A)K18 and (A)K19 were completely replaced after the 3rd sampling, *i.e.* after 282 days.

10⁻⁴ mol Br⁻ (kg H₂O)⁻¹ (Fig. 1). The effect of bromide on the release of Np, Pu, Tc and U became more significant, when the gas atmosphere was changed from an 8 vol. % H₂/92 vol. % Ar gas mixture to a pure Ar atmosphere in the 212–282 days interval. In the absence of hydrogen, concentrations of these redoxsensitive radioelements increased by a factor of 2.5 to 20 in experiment (A)K18, whereas in

experiment (A)K19 no significant change in their concentrations occurred (Fig. 1 and Table 1).

3.2 γ -radiation induced UO₂(s) corrosion

In the second type of experiments (cf. B), a maximum concentration of produced radiolysis gases was achieved after

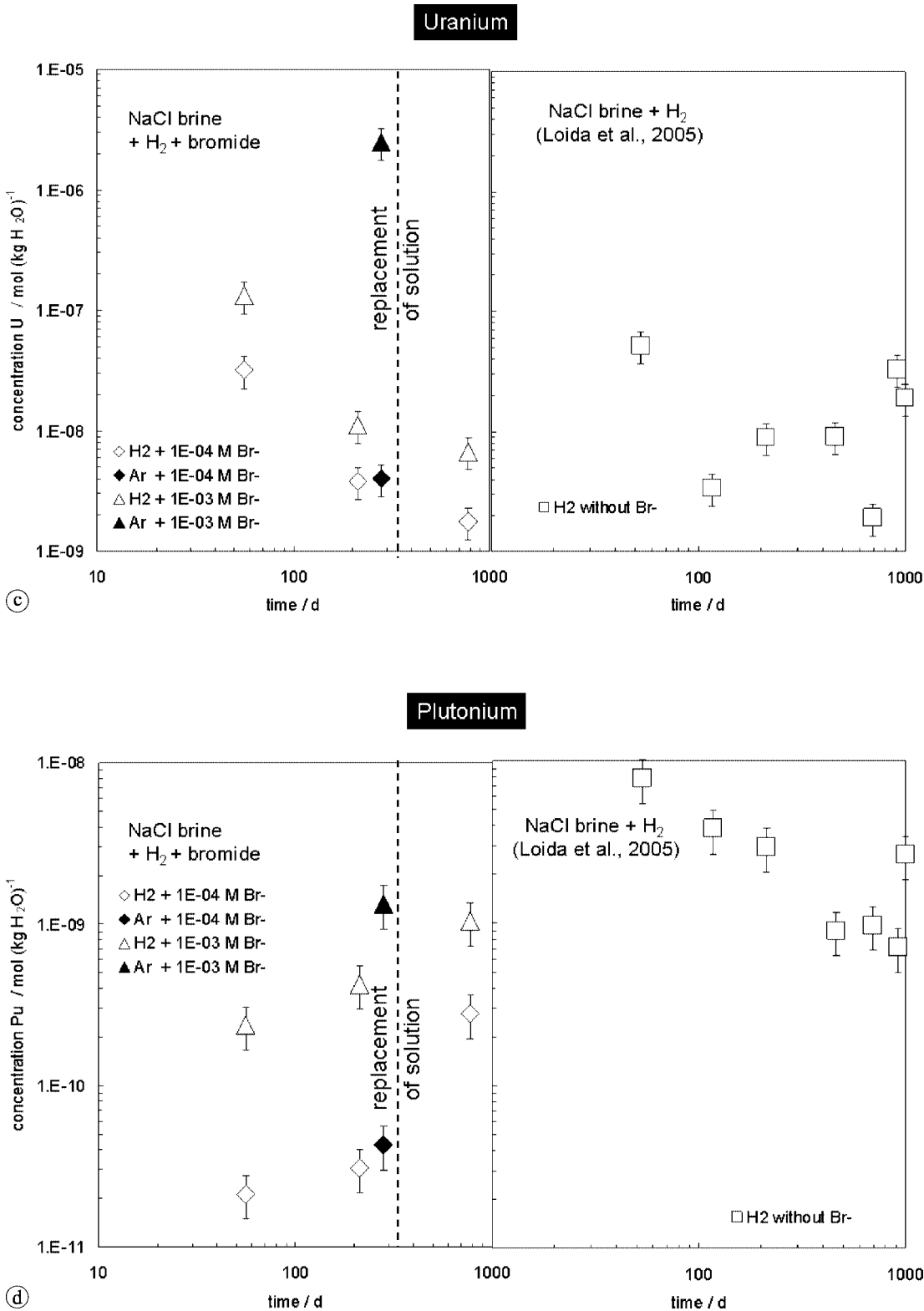


Fig. 1. Continued.

applying a γ -dose of > 1 MGy. Fig. 2 shows concentrations of dissolved H_2 and O_2 – the main long-lived radiolysis products – produced by γ -radiolysis of $6 \text{ mol (kg H}_2\text{O)}^{-1}$ NaCl solution as function of initial hydrogen and bromide concentrations. The range of hydrogen and bromide concentrations ($0\text{--}10^{-2} \text{ mol H}_2 \text{ (kg H}_2\text{O)}^{-1}$ and $0\text{--}10^{-3} \text{ mol Br}^- \text{ (kg H}_2\text{O)}^{-1}$) studied in our present and previously published [16] γ -radiolysis experiments covers the respective

concentrations of the SNF corrosion experiments. Since the maximum concentration in experiment (B)L1_06 does not represent a steady state value, maximum $\text{H}_2 + \text{O}_2$ concentrations of this experiment have a relatively high uncertainty. A comparison of results of (B)L1_06 ($10^{-3} \text{ mol H}_2 \text{ (kg H}_2\text{O)}^{-1}$) and (B)L2_06 ($10^{-3} \text{ mol H}_2 \text{ (kg H}_2\text{O)}^{-1} + 10^{-4} \text{ mol Br}^- \text{ (kg H}_2\text{O)}^{-1}$) with previous experiments on γ -radiolysis of $6 \text{ mol (kg H}_2\text{O)}^{-1}$ NaCl [8, 16] show that in

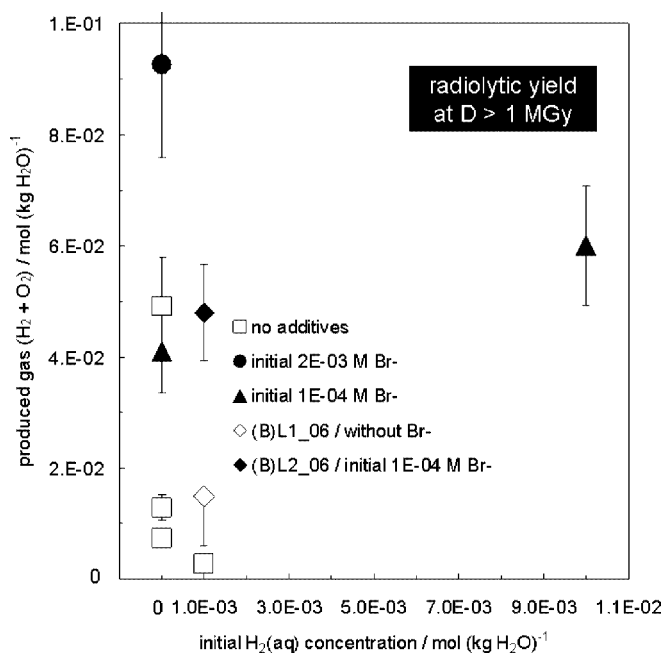


Fig. 2. Concentrations of gases ($\text{H}_2 + \text{O}_2$) produced by γ -radiolysis of 6 molal NaCl solution as function of initial concentrations of dissolved hydrogen and bromide. Open symbols denote results of experiments without bromide, and filled symbols denote those of experiments with an initial concentration of 10^{-4} to 2×10^{-3} molal Br^- . Data are derived from the study of Metz *et al.* [16].

presence of bromide, concentrations of H_2 and O_2 are significantly higher compared to their concentrations in experiments without bromide (Fig. 2). In contrast to the observed increase in the radiolytic yield due to the presence of bromide, no significant effect of Br^- on aqueous U concentration was observed under the studied conditions. During experiments (B)L1_06 and (B)L2_06, concentration of dissolved U reached within error the same concentration level (Table 1 and Fig. 3). Since U concentration was not monitored during irradiation, it is not evident if the final concentration of U represents a steady state concentration.

3.3 Detection of secondary phases in experiments on γ -radiation induced $\text{UO}_2(\text{s})$ corrosion

Aqueous U concentrations measured in the experiments on γ -radiation induced $\text{UO}_2(\text{s})$ corrosion agree well with the solubility limits of the meta-schoepite ($\text{UO}_3 \cdot 2\text{H}_2\text{O}(\text{cr})$)-Nadiuranate/clarkeite ($\text{NaUO}_2\text{O}(\text{OH})(\text{cr})$) transition (Fig. 3). These results are corroborated by results of AFM, EXAFS, SEM-EDS and XPS measurements, showing precipitates of secondary U(VI) phases on the pellets recovered from the γ -radiolysis experiments. As observed by means of AFM and SEM-EDS, the sample of experiment (B)L1_06 is covered completely by a $1 \mu\text{m}$ thick surface precipitate (with an atomic ratio $\text{U}/\text{Na} = 1.1 \pm 0.1$), whereas on the surface of the (B)L2_06 sample isolated particles of this U-Na phase ($\sim 0.5 \mu\text{m}$ in height) and few particles of a Na free uranium phase ($< 0.5 \mu\text{m}$ in height) are observed (Fig. 4). In blank experiment (B)LPI the concentration of dissolved U was more than two orders of magnitude lower than the U concentration in experiments (B)L1_06 and (B)L2_06, and equaling the solubility of $\text{U}(\text{OH})_4(\text{am})$ (Fig. 3). Moreover,

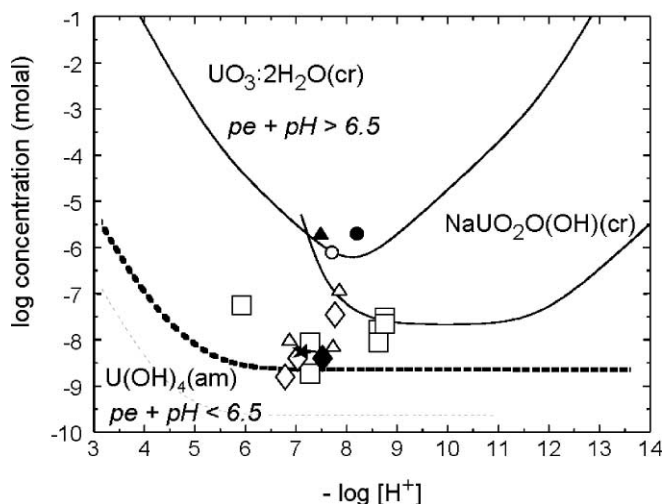


Fig. 3. Aqueous uranium concentrations measured in SNF/ $\text{UO}_2(\text{s})$ corrosion experiments under hydrogen overpressure compared to solubilities of $\text{U}(\text{OH})_4(\text{am})$, $\text{UO}_3 \cdot 2\text{H}_2\text{O}(\text{cr})$ and $\text{NaUO}_2\text{O}(\text{OH})(\text{cr})$ in $5.6 \text{ mol (kg H}_2\text{O)}^{-1}$ NaCl. $\text{U}(\text{OH})_4(\text{am})$ is stable at $pe + pH < 6.5 \pm 0.5$ whereas $\text{UO}_3 \cdot 2\text{H}_2\text{O}(\text{cr})$ and $\text{NaUO}_2\text{O}(\text{OH})(\text{cr})$ are stable at less reducing conditions. Symbols denote data of following experiments: Δ - (A)K18/SNF + H_2 + 10^{-3} M Br^- , \blacktriangle - (A)K18/SNF + Ar + 10^{-3} M Br^- , \diamond - (A)K19/SNF + H_2 + 10^{-4} M Br^- , \blacklozenge - (A)K19/SNF + Ar + 10^{-4} M Br^- , \square - SNF + H_2 (data of Loida *et al.* [7]), \circ - (B)L1_06/ γ -irradiated $\text{UO}_2(\text{s})$ + H_2 , \bullet - (B)L2_06/ γ -irradiated $\text{UO}_2(\text{s})$ + H_2 + 10^{-4} M Br^- , \star - non-irradiated blank experiment/ $\text{UO}_2(\text{s})$ + Ar.

the pellet recovered from experiment (B)LPI is characterized by a U(IV) surface composition according to XPS analyses (Fig. 5). The binding energy of the $\text{U} 4f_{7/2}$ elemental line of pellet (B)LPI is 380.0 eV. A shake-up satellite at a distance of 6.8 eV to the main line is observed, characteristic for U(IV)-oxide. Besides 4f elemental lines, XPS valence bands with the U 5f elemental line indicates the valency of uranium if compared to a $\text{UO}_2(\text{s})$ reference sample (CBNM#106, EC Reference Material no. 106 [21] fractured in the ultra high vacuum of the XPS). U(IV) contributes two 5f electrons per atom, U(V) one 5f electron and U(VI) results no 5f elemental line intensity (Fig. 5). The $\text{UO}_{2.1(2)}$ stoichiometry at the outermost surface of the (B)LPI sample demonstrates that a significant oxidation of the pellet due to contamination of atmospheric O_2 during the experimental run is excluded. Due to the results of the blank experiment it is concluded that oxidation of the pellets in experiments (B)L1_06 and (B)L2_06 is related to formation of oxidizing radiolysis species. The $\text{U} 4f_{7/2}$ elemental lines of the both pellets have a binding energy of 381.4 eV and two shake-up satellites at a distance to the main line of 4.3, 9.7 eV, and 4.0, 9.9 eV, respectively, characteristic for U(VI) compounds. Na 1s elemental lines have similar binding energies of about 1071.5 eV pointing to similar bonding. O 1s spectra of the irradiated pellets indicate the formation of hydroxides at their surfaces. Atomic concentrations determined by XPS indicate similar amounts of U and Na together with an about 5-fold higher oxygen atomic concentration, but traces of Cl only, indicating a clarkeite or Na-diuranate type stoichiometry $(\text{Na}(\text{UO}_2)\text{O}(\text{OH}) \cdot (\text{H}_2\text{O})_n)$ with $0 \leq n \leq 6$. *In vacuo*, dehydration occurs to some extent. At pellet (B)L1_06 the low full-width-at-half-maxima, FWHM, of the 4f lines indicate the presence of one dis-

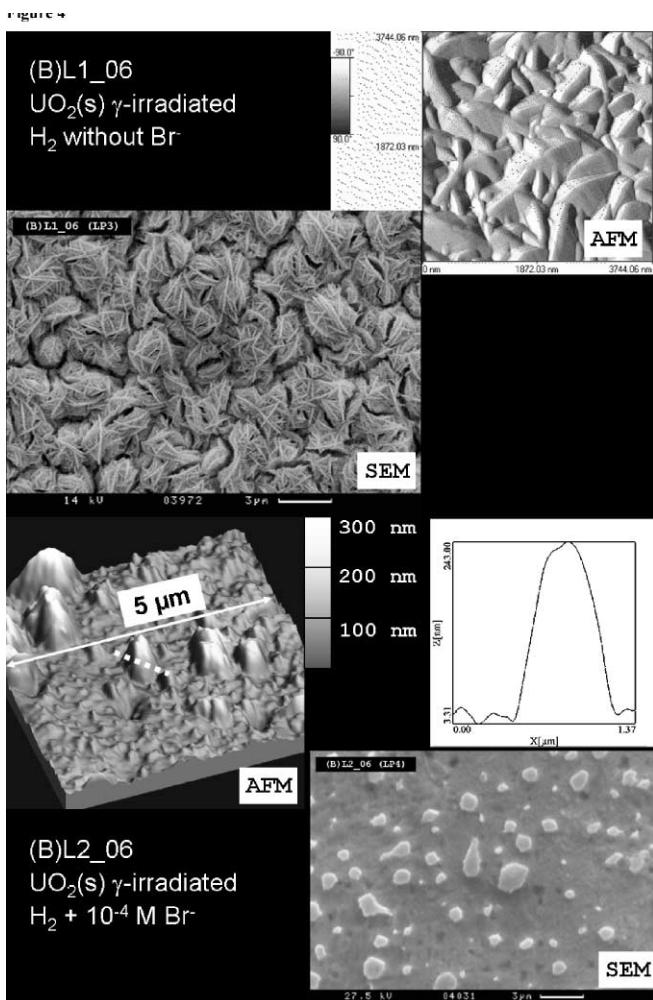


Fig. 4. AFM and SEM images of γ -irradiated $\text{UO}_2(\text{s})$ samples recovered from experiments (B)L1_06 and (B)L2_06. The exemplary height profile is taken from the section denoted by a stippled line in the AFM image of the (B)L2_06 sample.

tinct U compound at the pellet surface, in line with results of SEM-EDS.

EXAFS spectra of samples recovered from experiments (B)L1_06 and (B)L2_06 exhibit admixtures of surface precipitates with the underlying $\text{UO}_2(\text{s})$ bulk phase. Using 1-dimensional compound refractive lenses, the discrimination bulk/surface of the pellet recovered from experiment (B)L2_06 was improved, but not sufficiently to extract EXAFS information of the surface phase. From the XANES, it is clear that uranyl (UO_2^{2+}) is present on the surface as expected for clarkeite or meta-schoepite (Fig. 6). EXAFS fit analysis of the sample recovered from experiment (B)L1_06 identifies the surface precipitate as a clarkeite like phase.

4. Discussion

As will be discussed in the following, both types of experiments on α - β - γ - and γ -radiation induced $\text{UO}_2(\text{s})$ corrosion in NaCl brine under hydrogen overpressure show an influence of radiolysis on the stability of the $\text{UO}_2(\text{s})$ matrix and the release of certain radionuclides. Although these experiments were conducted in the presence of elevated concentrations of dissolved hydrogen, concentrations of the redoxsen-

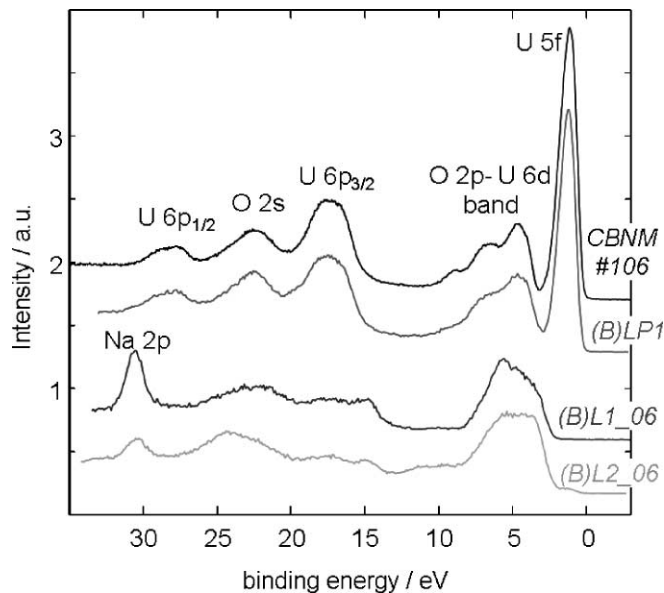


Fig. 5. XPS valence bands of $\text{UO}_2(\text{s})$ reference sample CBNM#106 fractured in UHV and of pellets recovered from the non-irradiated blank experiment (B)LP1 and the γ -radiolysis experiments (B)L1_06 and (B)L2_06. The U 5f elemental line indicates presence of U(IV).

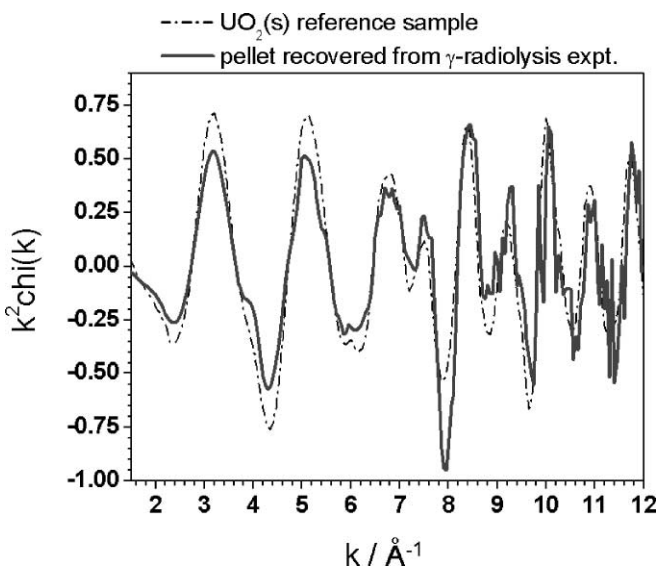


Fig. 6. k^2 -weighted U L_3 EXAFS of (B)L2_06 sample compared to an $\text{UO}_2(\text{s})$ reference sample.

sitive radioelements Pu and U were significantly higher than solubilities of the relevant Pu(IV) and U(IV) phases. In case of the γ -radiolysis experiments (B)L1_06 (H_2 without Br^-) and (B)L2_06 ($\text{H}_2 + 10^{-4} \text{ mol Br}^- (\text{kg H}_2\text{O})^{-1}$) it is evident from the aqueous concentration of U (Fig. 3) and from the composition of surface precipitates (Figs. 5–6) that the surfaces of the $\text{UO}_2(\text{s})$ matrix were oxidized to U(VI).

Pu and U release patterns in the SNF corrosion experiments (A)K18 and (A)K19 are not straightforward, showing a decrease in U and an increase in Pu concentrations with time. Fig. 3 shows aqueous U concentrations measured in both SNF corrosion experiments compared to solubilities of $\text{U}(\text{OH})_4(\text{am})$, $\text{UO}_3 \cdot 2\text{H}_2\text{O}(\text{cr})$ /meta-schoepite and $\text{NaUO}_2\text{O}(\text{OH})(\text{cr})$ /clarkeite in $5.6 \text{ mol } (\text{kg H}_2\text{O})^{-1}$ NaCl. Solubility data of U(IV) and U(VI) are derived

Table 2. Initial concentrations of dissolved H_2 and Br^- , final concentration of dissolved U, Cr, Fe, Ni, Mo, gases and final pH_c values of radiolysis experiments (B)L1_06, (B)L2_06 and of a blank experiment. Solution aliquots of experiments (B)L1_06 and (B)L2_06 were filtered by ultrafilters with 1.8 nm pore size. Due to the low yield in radiolysis gases, final gas composition in experiment (B)L1_06 is dominated by hydrogen added at the beginning of the experiment.

Experiment		(B)L1_06	(B)L2_06	blank
$C(H_2)_{initial}$	mol (kg H_2O) ⁻¹	1×10^{-3}	1×10^{-3}	0 (Ar)
$C(Br^-)_{initial}$	mol (kg H_2O) ⁻¹	0	1×10^{-4}	0
Duration	days	352	352	135
pH_c (final)		7.7	8.3	7.2
$C(U)_{final}/total$	mol (kg H_2O) ⁻¹	1×10^{-6}	4×10^{-6}	7×10^{-9}
$C(U)_{final}/ultrafil.$	mol (kg H_2O) ⁻¹	6×10^{-7}	2×10^{-6}	n.d.
$C(Cr)_{final}/ultrafil.$	mol (kg H_2O) ⁻¹	7×10^{-7}	1×10^{-4}	n.d.
$C(Fe)_{final}/ultrafil.$	mol (kg H_2O) ⁻¹	2×10^{-5}	1×10^{-5}	< d.l.
$C(Ni)_{final}/ultrafil.$	mol (kg H_2O) ⁻¹	8×10^{-5}	1×10^{-4}	n.d.
$C(Mo)_{final}/ultrafil.$	mol (kg H_2O) ⁻¹	2×10^{-5}	2×10^{-5}	n.d.
$X(H_2)_{final}$		90.5%	70.9%	n.d.
$X(O_2)_{final}$		9.5%	29.1%	n.d.
$X(CO_2)_{final}$		0%	0%	n.d.

from Refs. [22, 23]. $U(OH)_4(am)$ is stable at $pe + pH < 6.5 \pm 0.5$ (with respect to reaction $U(OH)_4(am) + 3H_2O = UO_3 \cdot 2H_2O(cr) + 2H^+ + 2e^-$) whereas $UO_3 \cdot 2H_2O(cr)$ and $NaUO_2O(OH)(cr)$ are stable at less reducing conditions. With exception of the relatively high U concentration measured in experiment (A)K18 under Ar atmosphere, concentrations of U are between the solubility limits of $UO_3 \cdot 2H_2O(cr)$, $NaUO_2O(OH)(cr)$ and $U(OH)_4(am)$. U concentrations measured at the beginning of experiments (A)K18 and (A)K19, *i.e.* 1×10^{-7} and 3×10^{-8} mol U (kg H_2O)⁻¹ respectively, correspond to the solubility of $NaUO_2O(OH)(cr)$ (Figs. 1 and 3). After 212 d, U decreased to levels of the $U(OH)_4(am)$ solubility, *i.e.* $10^{(-8.5 \pm 1.0)}$ mol (kg H_2O)⁻¹ according to thermodynamic data of Ref. [24]. Similarly, a slow decrease in U concentrations was observed in recent studies on SNF corrosion in 0.01 mol (kg H_2O)⁻¹ NaCl solution at 0.1 to 0.5 MPa H_2 and 25 °C [3, 25]. The authors of these studies interpreted the behavior of U as slow reduction of U(VI) to U(IV). In the 212 to 282 d interval of experiment (A)K18, the increase in the U concentration to the solubility limit of $UO_3 \cdot 2H_2O(cr)$ is directly related to the change of the gas composition from 4 MPa Ar/ H_2 to 0.1 MPa Ar, *i.e.* a change from strongly reducing to anoxic conditions. Neglecting the results of this anoxic stage, the decrease in U concentration may be interpreted as a slow reduction of pre-oxidized layers of the SNF pellets to U(IV), following the reasoning of [3]. Pu concentration in both SNF corrosion experiments increased with time (Fig. 1 and Table 1). Despite this increase, concentration of Pu in experiment (A)K19 ($H_2 + 10^{-4}$ mol Br^- (kg H_2O)⁻¹) was below the solubility limit of $Pu(OH)_4(am)$, which is $10^{(-10.4 \pm 0.5)}$ mol (kg H_2O)⁻¹ [24]. In experiment (A)K18 ($H_2 + 10^{-3}$ mol Br^- (kg H_2O)⁻¹), Pu concentrations after 282 d are significantly higher than the solubility of $Pu(OH)_4(am)$. One may consider either an oxidation of Pu(IV) to soluble Pu(V/VI) species or a reduction of Pu(IV) to soluble Pu(III) to explain the increase in Pu concentration. The assumption of an oxidation of Pu(IV) is supported

by two observations: (i) A considerable increase in Pu concentration is observed, when the experimental conditions changed from reducing to anoxic in the 212 to 282 d interval, and (ii) Pu concentrations are significantly higher in the experiment with the higher bromide concentration, *i.e.* (A)K18. On the other hand, in case of the proposed reduction of U(VI) to U(IV) a simultaneous reduction of Pu(IV) to Pu(III) is likely. Within the uncertainty of the thermodynamic data, measured concentrations of Tc and Np (Table 1) correspond to solubilities of $TcO_2 \cdot 1.6H_2O(s)$ and $Np(OH)_4(am)$, $10^{(-8.5 \pm 0.5)}$ and $10^{(-9.0 \pm 1.0)}$ mol (kg H_2O)⁻¹, respectively [24, 26–28]. Observed concentrations of Tc, Np, Pu and U are by several orders of magnitude above solubilities of the respective primary oxides, *i.e.* $TcO_2(c)$, $NpO_2(c)$, $PuO_2(c)$ and $UO_2(c)$.

For the interpretation of the current experiments in presence of bromide, we compare their results with results of a bromide free SNF corrosion experiment, “K8”, in 5.3 mol (kg H_2O)⁻¹ NaCl solution at 0.32 MPa H_2 overpressure, published by Loida *et al.* [7]. Except bromide concentrations, conditions in static stages of (A)K18 and (A)K19 were the same as in experiment “K8”. A relatively short washing cycle prior to the static stage of experiments (A)K18 and (A)K19 (*i.e.* two weeks) was carried out, whereas Loida *et al.* [7] removed the main part of the instant release fraction from the fuel pellet of “K8” in a wash procedure of totally 217 d, comprising six solution replacements. With the exception of the last samplings of experiments (A)K18 and (A)K19, Cs and Sr concentrations of these experiments were by ~ 1 order of magnitude higher than measured under bromide free conditions (Fig. 1). Concentrations of Pu and U observed at the end of experiments (A)K18 and (A)K19 were in the same range as those in the bromide free experiment (Figs. 1 and 3).

A pronounced effect of bromide on the radiolytic enhanced corrosion of the $UO_2(s)$ matrix is indicated by the release of Sr. For a variety of irradiated $UO_2(s)$ fuels, the release rate of Sr is considered as an indicator for the SNF

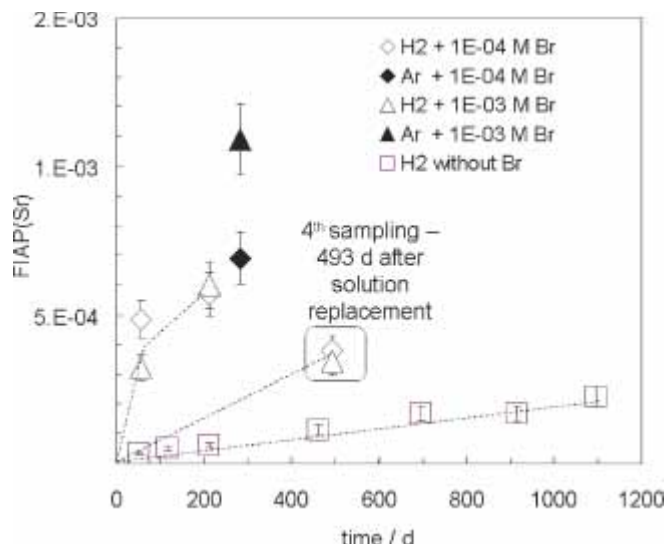


Fig. 7. Variation of FIAP(Sr) as function of time in SNF corrosion experiments (A)K18, (A)K19 (p.w.) and experiment “K8”, published by Loida *et al.* [7]. Symbols denote data of following experiments: Δ – (A)K18/SNF + H_2 + 10^{-3} M Br^- , \blacktriangle – (A)K18/SNF + Ar + 10^{-3} M Br^- , \diamond – (A)K19/SNF + H_2 + 10^{-4} M Br^- , \blacklozenge – (A)K19/SNF + Ar + 10^{-4} M Br^- . Solutions of both experiments were completely replaced 493 d before 4th. Stippled lines indicate the development of the Sr release between the various samplings.

matrix dissolution rate, because most of the Sr inventory is distributed homogeneously in the $\text{UO}_2(\text{s})$ matrix of the fuel, and Sr is scarcely involved in retention processes [29, 30]. As discussed in Ref. [29], previous corrosion experiments with samples of the same fuel rod used in the present study showed that initial Sr and U releases are rather similar (for instance initial U and Sr release rates of experiments “P56(I)” and “K9”, published in ref. [19]). Thus, it is concluded that the Sr inventory of the pellets used in the present experiments belongs mainly to the $\text{UO}_2(\text{s})$ matrix of the fuel. A continuous increase in Sr concentration with time is observed in SNF corrosion experiments (A)K18, (A)K19 and “K8” (Fig. 1). Sr concentrations in presence of bromide are significantly higher than under bromide free conditions. As an estimate for the Sr release rate, the gradient of FIAP(Sr) vs. time is calculated for each sampling according to

$$\text{FIAP}_{\text{Sr}} = \frac{A_{\text{aq}}(\text{Sr})V_{\text{solution}}}{A_{\text{SNF}}(\text{Sr})m_{\text{SNF}}} \frac{M(\text{UO}_2)}{M(\text{U})} \text{ and}$$

$$\frac{d\text{FIAP}_{\text{Sr}}(t)}{dt} = \left(\text{FIAP}_{\text{Sr}}(t) - \text{FIAP}_{\text{Sr}}(t-1) \left(1 - \frac{V_{\text{sample}}(t-1)}{V_{\text{solution}}(t-1)} \right) \right) \frac{1}{\Delta t}$$

where FIAP_{Sr} denotes Fraction of Inventory in the Aqueous Phase of Sr (dimensionless), $A_{\text{aq}}(\text{Sr})$ and $A_{\text{SNF}}(\text{Sr})$ the Sr activity (Bq) in solution and in spent nuclear fuel, respectively, V_{solution} the solution volume (L), V_{sample} the volume of the sampled aliquot (L), m_{SNF} the mass of fuel (g), $M(\text{UO}_2)$ and $M(\text{U})$ the molar weights of UO_2 and U (g mol^{-1}), t the sampling at time t and $(t-1)$ the previous sampling, and Δt denotes the time interval between two samplings (s). The variation of FIAP_{Sr} as a function of time in SNF corrosion experiments (A)K18, (A)K19 and in experiment “K8” are shown in Fig. 7. Since solutions of experiments (A)K18

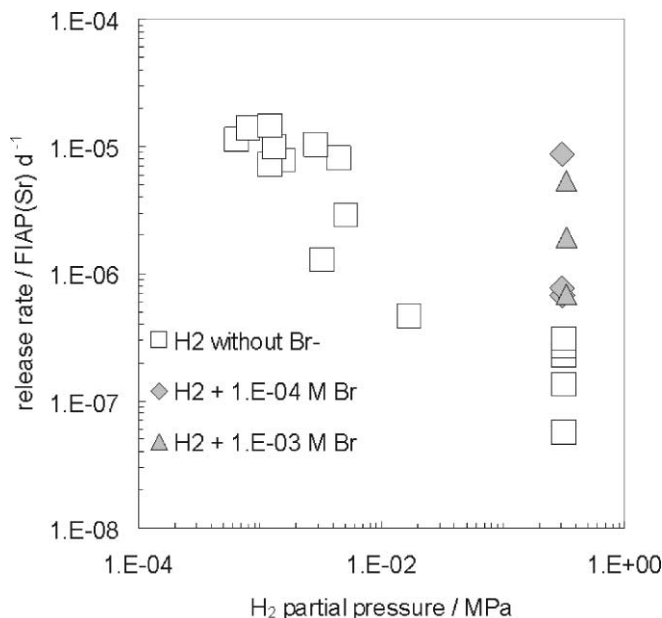


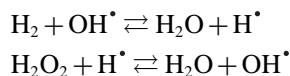
Fig. 8. Variation of Sr release rates (in terms of FIAP per day) as function of $P(\text{H}_2)$ in SNF corrosion in NaCl brine. Squares denote results of experiments in pure NaCl brine, derived from Loida *et al.* [7], diamonds and triangles denote those of experiments in NaCl brine containing 10^{-4} to 10^{-3} mol $(\text{kg H}_2\text{O})^{-1}$ Br^- , respectively.

and (A)K19 were completely replaced 493 d before the 4th sampling, a Sr free solution has to be considered for the interval Δt of this sampling, marked by the stippled line from the origin to the FIAP_{Sr} data at 493 days. In presence of bromide, both FIAP_{Sr} as well as gradients of FIAP_{Sr} vs. time were significantly higher compared to the respective values under bromide free conditions. Fig. 8 shows the variation of Sr release rates (in terms of FIAP_{Sr} per day) of experiments (A)K18, (A)K19 and “K8” as function of $P(\text{H}_2)$. Though the rates at 0.32 MPa $P(\text{H}_2)$ display a considerable scatter, it is obvious that in presence of 10^{-4} to 10^{-3} mol Br^- ($\text{kg H}_2\text{O})^{-1}$, the release of Sr was significantly enhanced. Similar to Sr release, the release of Cs from dissolving SNF was kinetically driven. In contrast to Sr, the Cs inventory is to a large extent associated to grain boundaries and the gap area of the pellets. An unambiguous quantification of the bromide effect on Cs release is not deduced, although relatively high Cs concentrations are observed in experiments (A)K18 and (A)K19 compared to experiment “K8” (Fig. 1).

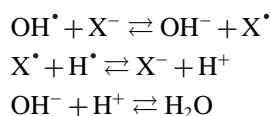
The observed relatively low concentrations of redox sensitive radioelements on one side and (fast) release of Sr and Cs on the other side are corroborated to some extent with results from recent SNF corrosion experiments in 0.01 mol dm^{-3} NaHCO_3 solution equilibrated with Ar/ H_2 gas (up to 30 vol. % H_2 /70 vol. % Ar at 0.1 MPa pressure) [31]. In their short term experiments, Eriksen and Jonsson [31] measured low concentrations of Tc ($\leq 10^{-10} \text{ mol dm}^{-3}$), U ($\leq 10^{-8} \text{ mol dm}^{-3}$), Np ($\leq 10^{-11} \text{ mol dm}^{-3}$) and Pu ($\leq 10^{-9} \text{ mol dm}^{-3}$) in presence of H_2 , whereas the observed release of Sr and Cs was not influenced by hydrogen.

Results of the SNF corrosion and the γ -radiolysis experiments in NaCl brine with elevated hydrogen concentrations and bromide concentrations of 0, 10^{-4} and 10^{-3} mol $(\text{kg H}_2\text{O})^{-1}$ indicate counteracting effects of H_2 and Br^-

on the production of radiolytic oxidants and the stability of the $\text{UO}_2(\text{s})$ matrix. The inhibition of SNF corrosion by dissolved hydrogen is related to a scavenging of radiolytic radicals by H_2 [1]. The role of hydrogen in the radiolytic reaction scheme is illustrated by following reactions of radiolytic H_2 and H_2O_2 with radicals OH^\bullet and H^\bullet ([15, 32] and references therein):



As a consequence, H_2 reduces the concentration of H_2O_2 by recombination to water. Relatively high concentrations of OH^\bullet and H^\bullet are produced in a low LET radiation field, whereas H_2O_2 is the main oxidizing radiolysis product in a high LET radiation field. In aqueous solutions containing $\geq 10^{-5}$ mol (kg $\text{Br}^- \text{H}_2\text{O}$) $^{-1}$ or high concentrations of chloride, the recombination of OH^\bullet and H^\bullet are catalyzed by these halogenides ($\text{X}^- = \text{Br}^-$ or Cl^-), rather than by H_2 and H_2O_2 ([15, 33, 34] and references therein):



Since the rate of reaction of OH^\bullet with Br^- or Cl^- is more than one order of magnitude faster than reaction $\text{H}_2 + \text{OH}^\bullet \rightleftharpoons \text{H}_2\text{O} + \text{H}^\bullet$, the scavenging effect of hydrogen with respect to OH^\bullet and H_2O_2 decreases with increasing halogenide concentration. The reaction of OH^\bullet with Br^- or Cl^- results to some extent in the production of oxo-halogenides (for example: $\text{OH}^\bullet + \text{X}^- \rightleftharpoons \text{XOH}^-$). Production of HClO , ClOH^- , ClO^- , HBrO and BrO^- had been measured in studies on α - and γ -radiolysis of aqueous NaCl and NaBr solutions [17, 33–35]. In experiments without hydrogen overpressure (radiolytic) oxidation of actinides by these oxo-chloride and oxo-bromide species had been observed [35–39]. In our γ -radiolysis experiments, the radiolytic production of hydrogen and oxygen was enhanced due to the presence of $\geq 10^{-4}$ mol (kg $\text{Br}^- \text{H}_2\text{O}$) $^{-1}$ (Fig. 2). Although the radiolytic yield was significantly less in experiment (B)L1_06 (H_2 , without Br^-) than in experiment (B)L2_06 ($\text{H}_2 + 10^{-4}$ mol (kg $\text{Br}^- \text{H}_2\text{O}$) $^{-1}$), concentrations of radiolytic oxidants were sufficient for oxidizing $\text{UO}_2(\text{s})$ to U(VI) . Radiolytic decomposition of NaCl brine in the SNF corrosion experiments (A)K18, (A)K19 and “K8” is reflected by the increase in hydrogen concentration (Table 1 and Ref. [7]). Concentrations of O_2 were below detection limit in these experiments, indicating that radiolytic oxygen was quantitatively consumed. The relatively low concentrations of redoxsensitive elements Np , Pu , Tc and U indicate that radiolytic oxidants (O_2 or oxo-halogenides) were quantitatively reduced in the SNF corrosion experiments. The observation of enhanced release of matrix bound elements (Sr , Np , Pu , Tc and U) during the anoxic interval (212 to 282 d) supports the interpretation that a reduction of radiolytic oxidants before 212 and after 282 d is directly related to the presence of hydrogen. Interfacial reactions at the SNF surface are proposed to explain the decrease in U concentrations and the consumption of radiolytic O_2 and other oxidants. In contrast to the γ -radiolysis experiments, the

γ -dose rate in the bulk of the SNF corrosion experiments is much less, whereas the ratio of $\text{UO}_2(\text{s})$ surface area to solution volume is about 40 times larger.

In the generalized “matrix alteration model”, MAM, dissolution and alteration of spent nuclear fuel under oxic and anoxic conditions is described as a sequence of radiolytic decomposition of the solution, oxidation of the $\text{UO}_2(\text{s})$ matrix, release of radionuclides and precipitation of secondary phases [4, 40, 41]. Based on results of the present study it is suggested that corrosion of the fuel’s $\text{UO}_2(\text{s})$ matrix, release of radionuclides, reduction of redox sensitive elements and consecutive precipitation of secondary phases occurs in solutions with sufficiently high chloride or bromide concentrations according to a MAM-type phenomenological reaction scheme, even under hydrogen overpressure:

- 1) Radiolytic decomposition of aqueous media and consecutive production of oxidants by radiolytic oxidation of chloride and bromide;
- 2) competitive reactions of OH^\bullet radicals with hydrogen, chloride and bromide and secondary radiolysis products;
- 3) oxidation of the $\text{UO}_2(\text{s})$ surface to soluble U(VI) , disintegration of the matrix and consecutive release of matrix bound radionuclides;
- 4) reduction and precipitation of redox sensitive radionuclides in spatial compartments with predominantly reducing conditions.

Proposing step (1) and (2) are based on results of present and published radiolysis experiments. The speculative steps (3) and (4) are reflected in the release of Sr , indicating the disintegration of the matrix, and the low concentrations of redox sensitive elements, interpreted as reduction processes. As discussed in Refs. [3, 6, 42], reduction of redox sensitive radionuclides is facilitated by processes at the fuel surface, whereas dissolved hydrogen is inert at room temperature in the absence of $\text{UO}_2(\text{s})$ or other catalytic surfaces. We argue that on the heterogeneous fuel surface exist compartments, where redox reactions with hydrogen are promoted and reducing conditions prevail. Studies on the corrosion of SIMFUEL and irradiated UO_2 fuel [43, 44] have shown that ϵ -phases exert a very significant effect on the corrosion behavior of the fuel. These metallic particles catalyze oxidation of hydrogen and reduction of oxidative radiolysis products, resulting in an inhibition of the $\text{UO}_2(\text{s})$ corrosion. In contrast to the present SNF corrosion experiments, γ -radiolysis experiments (B)L1_06 and (B)L2_06 were carried out using pellets of depleted $\text{UO}_2(\text{s})$, which did not contain any of these metallic particles. Consequently, no significant reduction of radiolytic oxidants and U(VI) are expected under the conditions of the present γ -radiolysis experiments.

5. Conclusions

Results of the complementary experiments on spent nuclear fuel corrosion and γ -radiation induced $\text{UO}_2(\text{s})$ corrosion in NaCl brine allow the conclusion that even trace concentrations of Br^- reduce the protective hydrogen effect with respect to the stability of the $\text{UO}_2(\text{s})$ matrix. Studied Br^- concentrations, 10^{-4} and 10^{-3} mol (kg H_2O) $^{-1}$, are relatively low with respect to brines of deep salt formations, however

in a range relevant for granitic and argillaceous groundwater. Low concentrations of Np, Pu, Tc and U indicate that retention processes such as precipitation of secondary phases control the release of the redox-sensitive radioelements rather than radiation induced corrosion processes. Unlike concentrations of actinides and Tc, concentration of dissolved Sr is kinetically controlled. Under hydrogen overpressure, the release rate of Sr is significantly enhanced in the presence of bromide. In a reaction scheme similar to the "matrix alteration model", we suggest that actinides and Tc are oxidized, and matrix bound radionuclides are released from the fuel matrix even under H_2 overpressure. In consecutive interfacial reactions redox sensitive radionuclides are reduced and precipitated. To test the MAM reaction scheme in presence of elevated hydrogen concentrations, future research activities may focus on the redox state of aqueous actinide species, released from dissolving spent nuclear fuel. For assessing the relevance of chloride and bromide for the long-term stability of SNF, further research is recommended to determine the influence of hydrogen, bromide and chloride on corrosion of SNF and α -doped $\text{UO}_2(\text{s})$ both in brines and in less concentrated aqueous solutions.

Acknowledgment. The authors would like to thank our colleagues at INE, in particular to N. Müller for his careful hot cell and glove box laboratory work, M. Fuss, F. Geyer, A. Goertzen, F. Heberling, S. Rabung and C. Walschburger for carrying out the AFM and (radio)chemical analyses, B. Brendebach, J. Römer, J. Rothe and E. Soballa for technical assistance during GI-XAFS and SEM-EDS analyses. J. Reinhardt and M. Dubiel (IOM, Leipzig, Germany) are acknowledged for their experimental work at the IOM GB77 γ -source. We are grateful to K. Spahiu for fruitful discussions regarding the impact of hydrogen and halogenides on radiolysis induced $\text{UO}_2(\text{s})$ corrosion. He helped considerably to improve the paper. The valuable comments of M. Kelm and B. Kienzler as well as thorough reviews by two anonymous reviewers are gratefully acknowledged. This study has been financially supported in part by the commission of the European Communities (Integrated Project NF-PRO, Contract FI16W-CT-2003-02389).

References

- Kelm, M., Bohnert, E.: A kinetic model for the radiolysis of chloride brine, its sensitivity against model parameters and a comparison with experiments. *Forschungszentrum Karlsruhe Wissenschaftliche Berichte, FZKA 6977* (2004), p. 60.
- Spahiu, K., Werme, L., Eklund, U.-B.: The influence of near field hydrogen on actinide solubilities and spent fuel leaching. *Radiochim. Acta* **88**, 507 (2000).
- Spahiu, K., Cui, D., Lundström, M.: The fate of radiolytic oxidants during spent fuel leaching in the presence of dissolved near field hydrogen. *Radiochim. Acta* **92**, 625 (2004).
- Bruno, J., Ewing, R. C.: Spent nuclear fuel. *Elements* **2**, 343 (2006).
- Ollila, K., Albinsson, Y., Oversby, V. M., Cowper, M.: Dissolution rates of unirradiated UO_2 , UO_2 doped with U-233, and spent fuel under normal atmospheric conditions and under reducing conditions using an isotope dilution method. SKB TR-03-13, Svensk Kärnbränslehantering AB, Stockholm, Sweden (2003), p. 35.
- Carbol, P., Spahiu, K., Cobos-Sabate, J., Glatz, J. P., Ronchi, C., Rondinella, V. V., Wegen, D., Wiss, T., Loida, A., Metz, V., Kienzler, B., Grambow, B., Quinones, J., Martínez-Esparza, A.: The effect of dissolved hydrogen on the dissolution of ^{233}U doped $\text{UO}_2(\text{s})$, high burn-up spent fuel and MOX fuel. SKB TR-05-09, Svensk Kärnbränslehantering AB, Stockholm (2005), p. 139.
- Loida, A., Metz, V., Kienzler, B., Geckeis, H.: Radionuclide release from high burnup spent fuel during corrosion in salt brine in the presence of hydrogen overpressure. *J. Nucl. Mater.* **346**, 24 (2005).
- Kelm, M., Bohnert, E.: Gamma radiolysis of NaCl brine: Effect of dissolved radiolysis gases on the radiolytic yield of long-lived products. *J. Nucl. Mater.* **346**, 1 (2005).
- Wittwer, C.: Sondierbohrungen Böttstein, Welach, Riniken, Schafisheim, Kaisten, Leuggern – Probennahmen und chemische Analysen von Grundwässern aus den Sondierbohrungen. NTB 85-49 report, NAGRA, Wettingen, Switzerland (1986).
- Ekberg, C.: Uncertainties in actinide solubility calculations illustrated using the Th-OH- PO_4 system. Ph. D. thesis, Chalmers University of Technology, Göteborg, Sweden (1999).
- Pearson, F. J., Arcos, D., Bath, A., Boisson, J.-Y., Fernandez, A. M., Gäbler, H.-E., Gaucher, E., Gautschi, E., Griffault, L., Hernan, P., Waber, H. N.: Mont Terri Project – Geochemistry of water in the Opalinus clay formation at the Mont Terri rock laboratory. Bundesamt für Wasser und Geologie, BWG, Bern (2003), p. 313.
- Herrmann, A. G., von Borstel, L. E.: The composition and origin of fluid inclusions in Zechstein evaporites of Germany. *Neues Jahrbuch für Mineralogie Monat.* (6), 263 (1991).
- Braitsch, O.: *Salt Deposits, Their Origin and Composition*. Springer Verlag, Berlin (1971), p. 297.
- Herrmann, A. G., Knipping, B.: Fluide Komponente als Teile des Stoffbestandes der Evaporite im Salzstock Gorleben. Technische Universität Clausthal (1993).
- Henglein, A., Schnabel, W., Wendenburg, J.: *Einführung in die Strahlenchemie*. Verlag Chemie GmbH, Weinheim (1969).
- Metz, V., Bohnert, E., Kelm, M., Schild, D., Reinhardt, J., Kienzler, B., Buchmeiser, M. R.: Gamma-radiolysis of NaCl brine in the presence of $\text{UO}_2(\text{s})$: Effects of hydrogen and bromide. *Mater. Res. Soc. Sci. Basis Nucl. Waste Management XXX* **985**, 33 (2007).
- Paviet-Hartmann, P., Hartmann, T.: Optimizing nuclear waste repository developments by implementing experimental data on radiolysis. in Int'l Conf. GLOBAL 2007 Nuclear Energy Systems for Future Generation and Global Sustainability, Boise, Idaho, USA (2007), pp. 691–695.
- Loida, A., Kienzler, B., Metz, V.: Alteration behavior of high burnup spent fuel in salt brine under hydrogen overpressure and in presence of bromide. *Mater. Res. Soc. Sci. Basis Nucl. Waste Management XXX* **985**, 14 (2007).
- Grambow, B., Loida, A., Martínez-Esparza, A., Díaz-Arocas, P., de Pablo, J., Paul, J.-L., Marx, G., Glatz, J.-P., Lemmens, K., Ollila, K., Christensen, H.: Long-term safety of radioactive waste disposal: source term for performance assessment of spent fuel as a waste form. Final report. Source term for performance assessment of spent fuel as a waste form. European Commission, Nuclear Science and Technology Series. Forschungszentrum Karlsruhe Wissenschaftliche Berichte, FZKA 6420 (2000), p. 202.
- Altmaier, M., Metz, V., Neck, V., Müller, R., Fanghänel, T.: Solid-liquid equilibria of $\text{Mg}(\text{OH})_2(\text{cr})$ and $\text{Mg}(\text{OH})_3\text{Cl}\cdot 4\text{H}_2\text{O}(\text{cr})$ in the system Mg-Na-OH-Cl- H_2O at 25 °C. *Geochim. Cosmochim. Acta* **67**, 3595 (2003).
- CBNM-Central-Bureau-for-Nuclear-Measurements: Certified Nuclear Reference Material, certificate of analysis of CBNM reference material no. 106. Joint Research Centre Geel Establishment (CBNM) (1984).
- Fanghänel, T., Neck, V.: Aquatic chemistry and solubility phenomena of actinide oxides/hydroxides. *Pure Appl. Chem.* **74**, 1895 (2002).
- Neck, V., Altmaier, M., Müller, R., Schlieker, M., Fanghänel, T.: Solubility of U(VI) in NaCl and MgCl_2 solutions. In 9th International Conference on Chemistry and Migration Behaviour of Actinides and Fission Products in the Geosphere, Migration '03, Gyeongju, Korea (2003).
- Neck, V., Kim, J. I.: Solubility and hydrolysis of tetravalent actinides. *Radiochim. Acta* **89**, 1 (2001).
- Ekeröth, E., Gransfors, M., Schild, D., Spahiu, K.: The influence of hydrogen on spent nuclear fuel dissolution. In: 11th International Conference on Chemistry and Migration Behaviour of Actinides and Fission Products in the Geosphere, Migration '07 (2007).
- Meyer, R. E., Arnold, W. D., Case, F. I., O'Kelley, G. D.: Solubility of Tc(IV) oxides. *Radiochim. Acta* **55**, 11 (1991).
- Eriksen, T., Ndalamba, P., Bruno, J., Caceci, M.: The solubility of $\text{TcO}_2\cdot n\text{H}_2\text{O}$ in neutral to alkaline solutions under constant p_{CO_2} . *Radiochim. Acta* **58**, 67 (1992).

28. Neck, V., Fanghänel, T., Metz, V., Kienzler, B.: Kenntnisstand zur aquatischen Chemie und thermodynamischen Datenbasis von Actiniden und Technetium. Bericht BfS-Projekt 9G213532100 (FZK-INE 001/01). (2001).
29. Grambow, B., Loida, A., Dressler, P., Geckeis, H., Gago, J., Casas, I., de Pablo, J., Giménez, J., Torrero, M. E.: Long-Term Safety of Radioactive Waste Disposal: Chemical Reaction of Fabricated and High Burnup Spent UO₂ Fuel with Saline Brines. Forschungszentrum Karlsruhe Wissenschaftliche Berichte, FZKA 5702 (1996), p. 174.
30. Grambow, B., Werme, L. O., Forsyth, R. S., Bruno, J.: Constraints by experimental data for modelling of radionuclide release from spent fuel. Proceedings of the International Symposium Basis for Nuclear Waste Management, Materials Research Society Vol. 176 (1990), p. 465–474.
31. Eriksen, T., Jonsson, M.: The effect of hydrogen on dissolution of spent fuel in 0.01 mol dm⁻³ NaHCO₃ solution. Svensk Kärnbränslehantering, SKB, Stockholm (2007), p. 19.
32. Pastina, B., LaVerne, J. A.: Hydrogen peroxide production in the radiolysis of water with heavy ions. *J. Phys. Chem. A* **103**, 1592 (1999).
33. Ershov, B. G., Gordeev, A. V., Kelm, M., Janata, E.: Radiation-chemical oxidation of bromide ions and formation of tribromide ions in weakly acidic aqueous solutions. *Mendeleev Commun.* **2001**(4), 149 (2001).
34. Ershov, B. G., Kelm, M., Janata, E., Gordeev, A. V., Bohnert, E.: Radiation-chemical effects in the near-field of a final disposal site: Role of bromide on the radiolytic processes in NaCl-solutions. *Radiochim. Acta* **90**, 617 (2002).
35. Büppelmann, K., Kim, J. I.: Chemical behaviour of plutonium in aqueous chloride solutions. RCM 01088. Technische Universität München, Germany, München (1988), p. 147.
36. Stadler, S., Kim, J. I.: Chemisches Verhalten von Americium in natürlichen wässrigen Lösungen: Hydrolyse, Radiolyse und Redox-Reaktionen. RCM 01188. Technische Universität München, Germany, München (1988), p. 141.
37. Magirius, S., Carnall, W. T., Kim, J. I.: Radiolytic oxidation of Am(III) to Am(V) in NaCl solutions. *Radiochim. Acta* **38**, 29 (1985).
38. Yusov, A. B., Shilov, V. P.: Photochemical oxidation of Am(III) in bicarbonate-carbonate solutions by BrO₃⁻, ClO₃⁻, and IO₃⁻. *Radiochemistry* **35**, 157 (1993).
39. Garnov, A. Y., Yusov, A. B., Shilov, V. P., Krot, N. N.: Reactions of hypobromite with neptunium(IV) and plutonium(IV) in alkali solutions. *Radiochemistry* **40**, 219 (1998).
40. Martínez-Esparza, A., Cunado, M. A., Cago, J. A., Quinones, J., Iglesias, E., Cobos, J., González de la Huebra, A., Cera, E., Merino, J., Bruno, J., de Pablo, J., Casas, I., Clarens, F., Giménez, J.: Development of a Matrix Alteration Model (MAM). Publicación técnica 01/2005, ENRESA, Madrid, Spain (2005), p. 101.
41. Poinssot, C., Ferry, C., Lovera, P., Jegou, C., Gras, J.-M.: Spent fuel radionuclide source term model for assessing spent fuel performance in geological disposal. Part II: Matrix alteration model and global performance. *J. Nucl. Mater.* **346**, 66 (2005).
42. Spahiu, K., Devoy, J., Cui, D., Lundström, M.: The reduction of U(VI) by near field hydrogen in the presence of UO₂(s). *Radiochim. Acta* **92**, 597 (2004).
43. Shoesmith, D. W.: Fuel corrosion processes under waste disposal conditions. *J. Nucl. Mater.* **282**, 1 (2000).
44. Shoesmith, D. W., Noel, J. J., Broczkowski, M. E., Goldik, J. S.: The influence of Epsilon particles on fuel corrosion/dissolution. In: International Spent Fuel Workshop, Uppsala, Sweden (2006).